The radiation impedance of the external ear of cat: Measurements and applications

J. J. Rosowski, L. H. Carney,[a,b] and W. T. Peake[a]
Research Laboratory of Electronics, Massachusetts Institute of Technology, 77 Massachusetts Avenue, Cambridge, Massachusetts 02139 and The Eaton–Peabody Laboratory, Massachusetts Eye and Ear Infirmary, 243 Charles Street, Boston, Massachusetts 02114

(Received 31 December 1986; accepted for publication 9 August 1988)

The configuration of external ears varies dramatically among mammalian species. In order to relate these structural differences to acoustic performance, it is useful to determine the "output" (radiation) impedance of the external ear. Measurements were made of the radiation impedance Z_E of the cat external ear looking out from the location of the tympanic membrane. Freshly excised external ears were coupled to a calibrated sound source at the tympanic ring, and the resulting sound pressure at the source was measured. The Z_E calculated from these measurements is masslike at frequencies below 2 kHz and approximately resistive above 4 kHz. The contributions of anatomically distinct sections of the external ear to Z_E were assessed by measuring the impedance before and after surgical removal of the pinna flange and of the concha. Mean measurements of the lengths and cross-sectional areas of components of the external ear are used in a simple model that consists of a uniform tube and an exponential horn; the radiation impedance of the model shows many of the features of the measured Z_E's. Measurements of the input impedance of the middle ear are combined with Z_E to infer the diffuse-field absorption cross section A_{DF}, which is a measure of the ear's performance as a coupler of acoustic power. It is suggested that A_{DF} is useful for across-species comparisons of the performance of external and middle ears.

PACS numbers: 43.63.Hx, 43.63.Th, 43.20.Rz, 43.80.Lb

INTRODUCTION

It is generally accepted that the external ears are the primary pathway through which sound signals are coupled from the environment into the middle ear of mammals (e.g., Shaw, 1974; Blauert, 1983). The enormous interspecies variations in the size and shape of mammalian external ears represent adaptations to different lifestyles and environmental needs (some of which may not be related to auditory performance[1]). Although measurements have been made of how the external ears affect the transmission of sound to the middle ear of various mammalian species (human: Shaw, 1974; cat: Wiener *et al.*, 1966; Phillips *et al.*, 1982; chinchilla: Von Bismark, 1967; Von Bismark and Pfeiffer, 1967; guinea pig: Sinyor and Laszlo, 1973; Drescher and Eldredge, 1974; mouse: Saunders and Garfinkle, 1982; bat: Lawrence and Simmons, 1982), the acoustic consequences of variations of external-ear size and shape have not been considered systematically. The large range of structural variations provides a natural opportunity to learn how the acoustic function of the external ear is related to structure.

To understand how external-ear structures affect acoustic function, we need measures of function that separate different aspects of the acoustic performance of the external ear, e.g., acoustic power collection and spatial selectivity, so that each aspect can be compared across species. Also, we need methods of separating the effects of different structures on the acoustic-performance measures. Acoustic performance of external ears has most often been described in terms of the ratio of pressure magnitudes, $|P_T(\phi,\theta)|/|P_{PW}|$—where $|P_T(\phi,\theta)|$, the magnitude of the sound pressure in the ear canal just lateral to the tympanic membrane, depends on the direction of the incident wave, as represented by the azimuthal and elevation angles, ϕ and θ, and $|P_{PW}|$ is the free-field sound-pressure magnitude of an incident uniform plane wave (Wiener and Ross, 1946; Wiener *et al.*, 1966; Shaw and Teranishi, 1968; Sinyor and Laszlo, 1973; Shaw, 1974; Mehrgardt and Mellert, 1977). Although this pressure ratio is a useful description of the operation of the ear as a sound receiver, for some purposes other measures are needed. (1) The pressure ratio depends on both the external and middle ears as well as the head[2]; methods are needed to separate the effects of these structures so that functional features can be related to particular structural features. (2) The ratio, by itself, does not determine power absorption by the middle ear. (3) The pressure ratio does not separate the spatial selectivity of the external ear from its power-collection performance.

Knowledge of the radiation impedance (or output impedance) of the external ear Z_E helps overcome these shortcomings. Although this impedance, which is observed by "looking out" through the external ear from the tympanic membrane (Fig. 1) has been determined for models of the human ear (Siebert, 1970, 1973; Shaw, 1976, 1982; Kuhn, 1979; Schroeter and Poesselt, 1986), few measurements for

[a] Also at: Department of Electrical Engineering and Computer Science, MIT, Cambridge, MA 02139.
[b] Present address: Department of Neurophysiology, University of Wisconsin—Madison, 1300 University Ave., Madison, WI 53706.

 0001-4966/88/111695-14$00.80

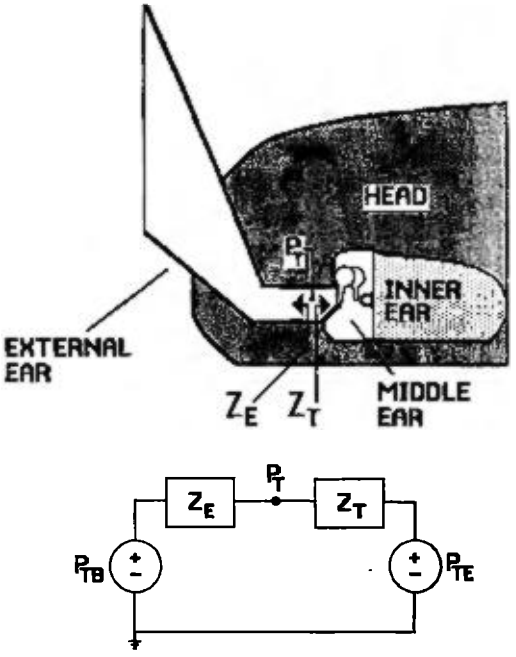

FIG. 1. A schematic cross-section through an ear that illustrates Z_E and Z_T as the acoustic impedances "looking out" and "looking in," respectively, from a point in the ear canal just outside the tympanic membrane. The equivalent circuit includes two sound-pressure sources in series with Z_E and Z_T. The Thévenin equivalent pressure, P_{TB}, for external sound sources is the sound pressure just outside the tympanic membrane when the membrane is blocked (i.e., $Z_T \rightarrow \infty$); P_{TE}, the Thévenin equivalent pressure for internal sources (e.g., otoacoustic emissions) is the sound pressure just outside the tympanic membrane when the ear canal is blocked (i.e., $Z_E \rightarrow \infty$). The net pressure at the tympanic membrane produced by both external and internal sources is P_T.

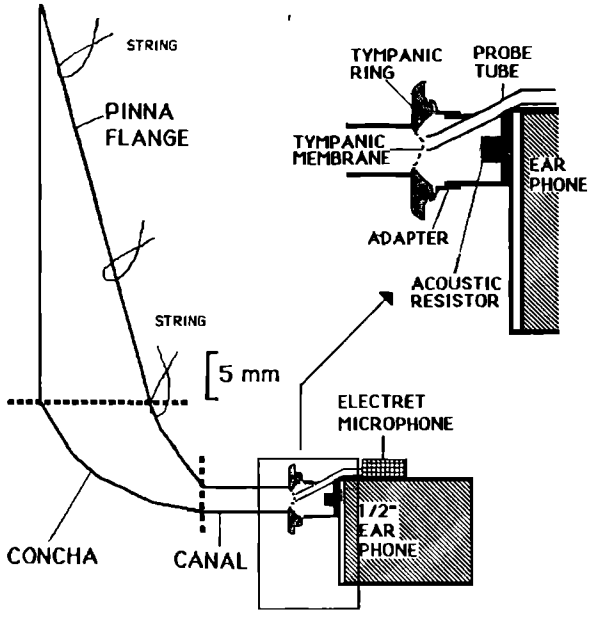

FIG. 2. A schematic representation of a cat external ear coupled to the impedance-measurement system. The thick dashed lines separate the three components of the external ear, the *Pinna flange*, *concha*, and *canal*. The strings, which supported the ear, were attached to a rigid frame. Components of the impedance-measurement system are labeled. The acoustic resistor (Knowles #BF-1923) has a nominal resistance of 470 mks acoustic MΩ. The electret microphone is a Knowles EA-1842, and the earphone is a Bruel & Kjaer condenser microphone (#4134). The inset shows the connection between the tympanic ring and acoustic system in more detail. The adapter fit snugly to a bony flange around the medial side of the tympanic ring. The dotted line near the opening of the probe tube shows the position of the tympanic membrane before it was removed.

real ears of any species (Rosowski *et al.*, 1986; Dear, 1987) have been reported previously. In this article we report measurements of Z_E in cat.

Knowledge of Z_E enables several useful computations. (1) Since Z_E is the output impedance of the external ear, we can use it with measurements of the input impedance of the middle ear Z_T (Fig. 1) to determine the effects of each impedance on sound pressures in the ear canal caused by both external and internal (e.g., Zurek, 1985) sound sources. (2) Through the reciprocity principle, we can use Z_E to determine the spatial average of the pressure ratio at the blocked tympanic membrane (Siebert, 1970, 1973; Shaw, 1976, 1988). (3) The reciprocity principle also allows us to determine the diffuse-field absorption cross section A_{DF} (a measure of the effectiveness of the ear in collecting acoustic power) from measurements of Z_E and Z_T (Shaw, 1979, 1988; Shaw and Stinson, 1983). This power-collection performance can be compared with that of an ideal receiver. Finally, we suggest an approach that may make it easier to obtain measurements from a variety of species, so that the acoustic behavior of a wide range of external-ear configurations can be compared.

I. METHODS

A. Preparation of the external ears

Most of the measurements presented in this article were made in six freshly excised ears from three cats. Each cat was anesthetized, and the muscles surrounding the external ear were detached from their insertions so as to expose the cartilaginous ear canal and its attachment to the bony tympanic ring. The animal was then sacrificed and the bone around the tympanic ring was chipped away so that the intact ring remained attached to the ear canal. The tympanic membrance was removed.

The first ear excised from each cat was immediately (within 20 min) suspended by strings in a support frame, and a tubular adapter was used to connect the medial side of the tympanic ring and the impedance measurement system (Fig. 2). The adapter was fashioned from nylon ("heat-shrink") tubing so that it fit snugly around both the circular output port of the sound system on one end and the elliptical bony ridge of the tympanic ring on the other end. The adapter provided an acoustically tight and mechanically secure coupling between the tympanic ring and the sound source. Since the cartilaginous walls of the external ear maintain their shape after excision, it was relatively easy to suspend the ear in its "natural position" on the support frame. Control measurements indicated that the radiation impedance of the external ear was not sensitive to small modifications in the suspension of the pinna or attachment to the sound source. After impedance measurements were made on the intact ear, the pinna flange (Fig. 2) was surgically removed, and the impedance was measured again. A third impedance measurement was made after removing the concha so that only the tubelike canal (Fig. 2) remained. The sec-

ond ear from each cat was excised while measurements were performed on the first ear. If necessary, the second ear was kept in refrigerated saline for a short time (30–60 min) while the measurements on the first ear were completed.

B. Measurement of acoustic impedance

The acoustic-impedance measurement method has been described previously (Lynch, 1981; Rosowski *et al.*, 1984). The sound pressures produced by a high-impedance sound source in two "known" acoustic loads (a 5-mm^3 cylindrical cavity and an acoustic transmission line[3]) were used to determine the Norton-equivalent volume velocity U_S and impedance Z_S of the sound source (Fig. 3). With the equivalent source parameters determined, measurements of sound pressure P_L in unknown acoustic loads were used to determine the acoustic impedance of the loads:

$$Z_L = (U_s/P_L - 1/Z_S)^{-1}. \quad (1)$$

The accuracy of the measurement technique was tested by measuring the impedance of several other "known" acoustic loads (Lynch, 1981; Rosowski *et al.*, 1984). Two of these tests are illustrated in Fig. 4, which compares the measured impedance of two loads (a circular opening in an "infinite baffle" and a rigid cylindrical cavity) with theoretical expressions for their load impedances. There is good agreement between the measured and theoretical impedances; the difference in magnitude between measurement and theory is less than 10% for the baffle and generally less than 20% for the cavity measurement (at frequencies near the cavity-impedance minimum, the difference between measurement and theory is larger). The difference between the measured and theoretical angle is less than 0.01 periods for frequencies between 0.2 and 7 kHz. The range of the magnitude of the ear-canal radiation impedance (Z_E in Fig. 4) is within the range of magnitudes of the two test impedances, and our measurements of Z_E should be as accurate as our measurements of the test loads.

Some external- and middle-ear performance characteristics (see Sec. III) depend on the real part of the radiation impedance, $\mathrm{Re}\{Z_E\} = |Z_E| \cos$ (Z_E angle). The accuracy of our $\mathrm{Re}\{Z_E\}$ estimates is highly dependent upon the Z_E angle and the accuracy of the angle measurements. When the angle is between ± 0.1 periods—as Z_E angle is between 2.5 and 10 kHz (Figs. 4 and 6)—an error of 0.01 periods leads to an error of less than 5% in the real part. The error in $\mathrm{Re}\{Z_E\}$ is much larger as the angle nears ± 0.25 periods; e.g., when the angle is 0.2 periods, the error in $\mathrm{Re}\{Z_E\}$ is as large as 25%. Because of this problem, we do not report measurements of $\mathrm{Re}\{Z_E\}$ when the angle of the impedance is close to ± 0.25 periods.

To determine whether impedance measurements remained stable over the 2- to 3-h period required for all the

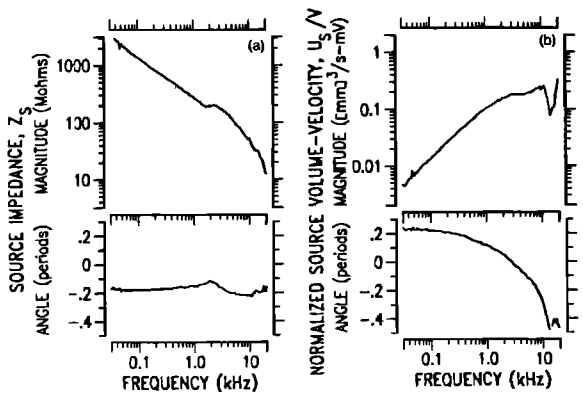

FIG. 3. Typical characteristics of the acoustic source determined from measurements in "known" loads. (a) The magnitude and angle of the equivalent source impedance Z_S. For stimulus frequencies below 1 kHz, the impedance is primarily determined by the air volume within the source; above 1 kHz, the acoustic resistor (Fig. 2) decouples the air volume adjacent to the earphone diaphragm. The units of impedance magnitude are mks acoustic megohms ($1\Omega = 1$ Pa-s/m^3 $= 1$ N-s/m^5). (b) The magnitude and angle of the normalized volume-velocity output U_S/V of the equivalent source; V is the voltage input to the earphone amplifier (nominal gain = 100). In this and all subsequent figures, measurements were made at 40 points per decade and are connected by straight lines.

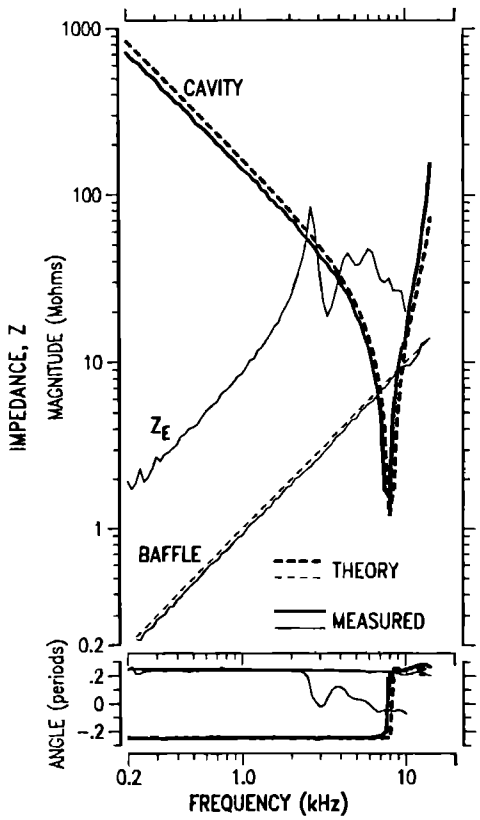

FIG. 4. Measurements of the acoustic impedance of test loads, including the radiation impedance of a round hole in a baffle, and the input impedance of a rigid cylindrical cavity. The baffle measurement was made with a 2-mm-thick aluminum plate, 0.6 m^2 in area, coupled to the sound source so that the opening of the sound measuring probe tube was flush with the outer surface of the plate. For the frequency range of interest, the load on the acoustic source with the baffle in place is the radiation impedance of a massless piston in an infinite baffle (Beranek, 1954, p. 118). The cylindrical cavity load had a diameter of 4 mm (identical to the sound port's inner diameter), was 10.5 mm long, and was machined to fit tightly to the impedance-measurement system. The solid lines are the measured impedances and the dashed lines are the theoretical impedances. The measured radiation impedance of a cat external ear Z_E is also shown. In the angle plot, the dashed lines (theory) are superposed on the corresponding solid lines over much of the frequency range.

measurements, repeated measurements were made on one ear over 6 h. Only small changes in Z_E occurred during that time. The magnitude of the impedance at 0.5 kHz increased by less than 1%, and the frequency of the $|Z_E|$ maximum ($\approx$2.8 kHz) decreased by less than 2%. The largest changes in Z_E occurred at frequencies between 5 and 10 kHz, where the average changes in Z_E magnitude and angle were 12% and 0.02 periods, respectively.

The measurements were made in a sound-insulated chamber (Vér *et al.*, 1975) with inside walls that are not particularly sound absorbent. The close match between the measured and theoretical "baffle" impedance (Fig. 4) indicates that room reverberations do not contribute significantly to the Z_E magnitude and angle measurements. Also, since, at frequencies above 2 kHz, the relatively small real part of the "baffle" impedance is generally within 40% of the theoretical value for radiation into an infinite half-space, reflections do not have a large effect on the real part measurements. Another test for possible influences of room reverberations consisted of measurements made with and without heavy cloth curtains placed about halfway between the ear and the walls. The curtains had no measurable effect on the magnitude, angle, or real part of Z_E.

C. Frequency limits of Z_E measurements

Sound-pressure measurements were performed under computer control. Tone frequency was stepped from 0.01 to 50 kHz at a density of 40 points per decade. Measurements were made with a fixed voltage into the earphone (the voltage was chosen so that the largest pressures produced were about 70 dB SPL, Fig. 5). With constant earphone voltage, the source volume velocity is smallest at low frequencies [Fig. 3(b)], where the impedance magnitude of the external ear is also small. Consequently, the sound pressure produced at frequencies below 0.2 kHz were too small to measure accurately (i.e., pressure magnitudes were within 10 dB of the noise floor, Fig. 5). Therefore, we present results only for frequencies above 0.2 kHz.

The high-frequency measurement limit results from nonuniformities in the sound presure in the ear tube. In calculating the radiation impedance of the external ear from a pressure measured at a point near the tympanic ring, we assume that the measurement is representative of the pressure averaged over the entire canal cross section. As has been discussed by Stinson (1985), this assumption is valid only below some high-frequency limit. An empirical determination of this limit was made with the aid of a "movable" probe tube. With an excised canal attached to the measurement system, a separate high-impedance probe-tube microphone—mounted on a micromanipulator—was inserted into the canal through a small hole in the tubular adapter (Fig. 2). The micromanipulator was used to move the probe transversely through the center of the canal from one wall to the other. The axis of probe motion paralleled the plane of the tympanic ring and came near the opening of the "stationary" probe tube of the acoustic system. Sound-pressure measurements were made at six locations within the cross section of the canal (inset of Fig. 6). The position of the movable probe had little effect on pressures measured with the stationary probe. Normalized measurements from the movable probe are shown in Fig. 6. At frequencies below 10

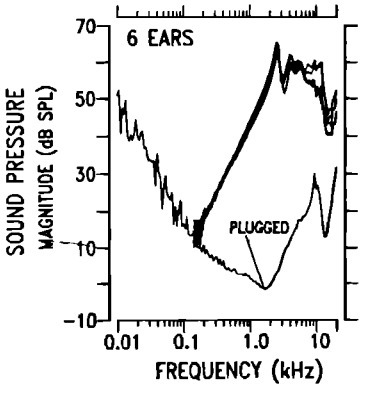

FIG. 5. The measured sound-pressure magnitudes used to compute the radiation impedances of the six external ears are compared with the noise floor of the measurement system obtained with the probe tube plugged with plasticene. The voltage into the earphone driver amplifier (nominal gain = 100) was 4.5 mV rms. Below 0.1 kHz, the pressures measured in the ear canal are not plotted because they are indistinguishable from the plugged measurements. All measurements were made with the aid of a tunable 2-Hz "tracking filter."

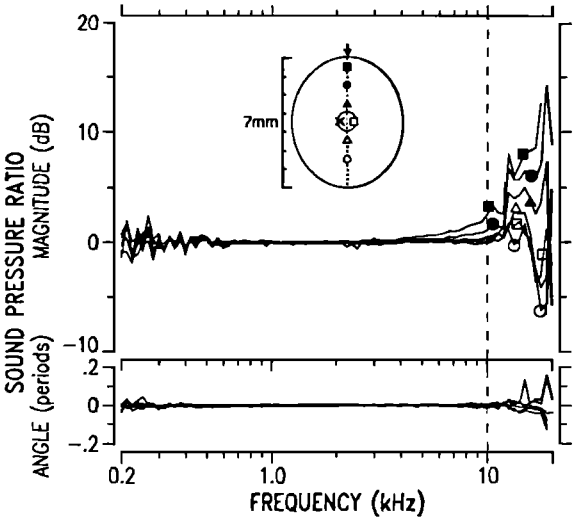

FIG. 6. Normalized sound pressures measured with the movable acoustic probe. Seven pressure measurements were made in the plane of the stationary probe tip of the impedance measurement system along a line perpendicular to the long axis of an attached canal. The measurement locations are schematized in the inset. The tympanic ring and the adjacent adapter are elliptical with a long axis of about 7 mm. The stationary probe of the impedance measurement system is in the center of the ellipse. Each symbol designates a different measurement. The first measurement of the series, ■, was made with the probe about 0.5 mm inside the edge of the adapter. The next five measurements were made after inward steps of 1 mm in probe position and the last measurement, □, was made after a step backward of 2 mm. The six curves show the pressure measured at six locations, normalized by the first pressure measurement made at the center, ×. The irregularities at the lowest frequencies result from the decreased signal-to-noise ratio at those frequencies (Fig. 5). The dashed vertical line marks 10 kHz, the frequency above which differences in magnitude of more than 3 dB occur.

kHz, the variation in pressure magnitude across the ear canal is less than 3 dB, and the variation in pressure angle is less than 0.02 periods. Because of the larger deviations in the pressure at higher frequencies, we report impedance measurements only for frequencies below 10 kHz.

D. Castings of the canal and concha

The structure of the cat's external ear is complicated, with (1) a sharp bend in the cartilaginous ear tube[4] at the canal–concha border, (2) abrupt changes in cross-sectional area, and (3) knobs and valleys on the inner and outer surface of the concha where the muscles that control pinna movement insert. To describe the configuration of the ear tube, each of the surgically separated canals and conchas was filled with a silastic casting material immediately after the impedance measurements were made. After the silastic had cured, the castings were removed. Most of the anatomical measurements we report were made from these castings.

II. RESULTS

A. External-ear dimensions

We divided the cat's external ear into three parts [Fig. 7(a); footnote 5]. The most peripheral component, the "pinna flange," was separated from the rest of the ear with a horizontal section at the inferior edge of the ear opening. The "concha" was separated from the more medial "canal" with a vertical cut at the point where the cartilaginous tube bends.

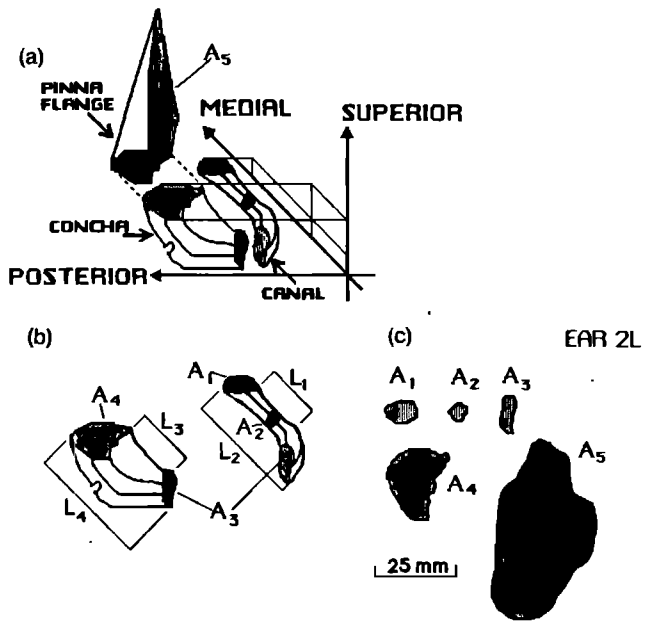

FIG. 7. Illustrations of external-ear anatomy and dimensions. (a) A perspective presentation of the three components of a right external ear showing the pinna flange, concha, and canal slightly displaced from each other. The lighter shading represents the planes of the observable openings of the three tubes. The darker shading represents planes hidden from view. In the pinna flange, there is a region of overlap of dark and light. The notch in the concha is a regular feature; a muscle normally inserts at this location. (b) Definition of the measured areas and lengths of the canal and concha (Table I). (c) Representative cross sections of the canal, concha (from ear 2L), and pinna-flange openings.

This is also the location of a natural "joint" in the tube; peripheral to this joint, the cross-sectional area of the tube increases rapidly.

At the junction between the canal and concha [A_3 in Fig. 7(b) and (c)], the cross section of the canal is oblong in shape, with the short axis horizontal. The cartilaginous ear tube easily flexes about the vertical axis of this canal–concha joint, which allows the concha and pinna flange to rotate so that the cat can change their spatial orientation with respect to the head.

Four measurements of linear dimensions of the canal and concha molds were made with calipers [Fig. 7(b)]: L_1, the minimum distance between the medial and lateral ends of the canal; L_2, the maximum canal length; L_3, the chord of the shorter arc of the concha; and L_4, the chord of the longer arc. With a camera lucida, magnified (5×) outlines of the flat surfaces of the ends of the molds were made [Fig. 7(c)] and were used to estimate areas. Four areas were measured: A_1, the area of the opening of the canal at the tympanic ring; A_2, the minimum cross-sectional area of the canal; A_3, the cross-sectional area at the canal–concha boundary; and A_4, the area of the concha opening. Estimates of the area of the pinna–flange opening, A_5, were made from metal castings of ears from two other cats (Wiener *et al.*, 1966). The results of these measurements, which are summarized in Table I, show some features in common with Shaw's (1974, p. 478) measurements of cat external ears and are used later in our development of a model of the external ear.

Repeated measurements of the same anatomical structures indicated measurement errors of as much as 10%. These relatively large errors result from subjective estimates involved in all of the anatomical measurements including the precise locations of planes of section and the definition of minimum and maximum dimensions.

The three cats were selected for their different body weights (1.9, 2.9, and 3.7 kg), and we looked for correlations between weight and the anatomical measurements. Only A_2 was significantly correlated (correlation coefficient of 0.9) with weight.

TABLE I. External-ear dimensions: Mean cross-sectional areas and lengths [see Fig. 7(b) and (c) for definitions].

Cross-sectional areas (mm^2)	N	Mean	± s.d.	Model[a,b]
A_1, Canal, medial opening	6	40	± 3	
A_2, Canal, minimum	6	19	± 2	20 (5)
A_3, Canal–concha boundary	6	37	± 8	
A_4, Concha—pinna-flange boundary	6	232	± 38	205 (16)
A_5, Pinna-Flange opening	2	1265	± 292	1280 (40)

Lengths (mm)		N	Mean	± s.d.	Model[a]
L_1, Canal,	minimum	6	9.5	± 1.3	
L_2,	maximum	6	18.9	± 1.5	14.5
L_3, Concha,	minimum	6	12.9	± 2.9	25
L_4,	maximum	6	25.4	± 1.7	

[a] The model, which is made up of a cylindrical tube and an exponential horn, is described in Sec. III.
[b] The diameter (in mm) is in parentheses.

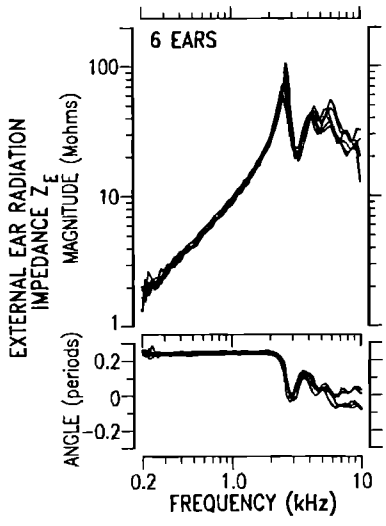

FIG. 8. The radiation impedance, magnitude, and angle of the six external ears from three cats. The units of impedance magnitude are mks megohms. Features of these measurements are presented in Table II.

B. Radiation impedance of the external ear Z_E

The magnitudes and angles of the radiation impedances of six external ears are illustrated in Fig. 8, and features of these measurements are tabulated in Table II. Despite differences in animal size, the six Z_E's are very similar; the range of the magnitudes and angles over the 0.3- to 2.35-kHz range is less than 20% and 0.05 periods, respectively. At frequencies below 2 kHz, Z_E is masslike, with a magnitude proportional to frequency and an angle near 0.25 periods. The magnitude of the impedance at 0.5 kHz ($|Z_E|_{0.5\,\mathrm{kHz}}$) varies between 4.1 and 4.6 MΩ. At frequencies above 4 kHz, Z_E is approximately resistive with a roughly constant magnitude of $\approx$30 MΩ and an angle near 0. In the middle-frequency range, each $|Z_E|$ has a maximum near 2.6 kHz ($f_{\max}$), a minimum near 3.2 kHz ($f_{\min}$), and the angle varies between 0.25 and -0.1 periods. The most variable features of the curves are the maximum impedance magnitude ($|Z|_{\max}$), which ranges from 65 to 114 MΩ, and the $Q_{3\,\mathrm{dB}}$ of the maximum ($Q_{\max}$) which ranges from 4.9–14.3.

Correlation coefficients were computed between the features in Table II and animal weight. The features that describe the impedance maxima and minima ($f_{\max}$, $|Z|_{\max}$, $Q_{\max}$, and $f_{\min}$) all show a tendency to correlate negatively with body weight (with correlation coefficients of 0.76, 0.74, 0.80, and 0.85, respectively). However, only the correlation between weight and $f_{\min}$ is significant at the 5% level.

TABLE II. Features of the radiation impedance Z_E: Measurements and model.

	Ear[a]							
	1R	1L	2R	2L	3R	3L	Mean ± s.d.	Model[b]
Intact ear								
$\lvert Z\rvert_{0.5\,\mathrm{kHz}}$ (MΩ)	4.2	4.6	4.2	4.5	4.1	4.2	4.30 ± 0.20	4.9
$\lvert Z\rvert_{\max}$ (MΩ)[c]	65	85	85	63	95	114	84.5 ± 18.8	222
$f_{\max}$ (kHz)[c]	2.53	2.67	2.61	2.52	2.71	2.70	2.62 ± 0.08	2.87
$Q_{\max}$[d]	6.2	9.3	8.8	4.9	11.2	14.3	9.12 ± 3.39	14.2
$f_{\min}$ (kHz)[e]	3.19	3.21	3.21	3.22	3.36	3.38	3.26 ± 0.08	3.62
Canal and concha								
$\lvert Z\rvert_{0.5\,\mathrm{kHz}}$ (MΩ)	4.2	4.4	4.4	4.5	4.0	4.2	4.28 ± 0.18	4.8
$\lvert Z\rvert_{\max}$ (MΩ)	195	140	192	193	177	145	173 ± 25.0	1134
$f_{\max}$ (kHz)	3.22	3.22	3.00	3.26	3.26	3.35	3.22 ± 0.12	3.20
$Q_{\max}$	14.0	12.6	12.6	12.9	13.0	9.1	12.4 ± 1.68	56.1
$f_{\min}$ (kHz)	4.35	4.12	4.11	4.35	4.35	4.34	4.27 ± 0.12	4.89
Canal only								
$\lvert Z\rvert_{0.5\,\mathrm{kHz}}$ (MΩ)	3.0	3.2	3.0	3.2	2.9	3.0	3.05 ± 0.12	3.1
$\lvert Z\rvert_{\max}$ (MΩ)	301	230	375	286	344	398	322 ± 62.1	1533
$f_{\max}$ (kHz)	5.51	5.55	4.87	5.08	5.46	5.73	5.37 ± 0.33	5.39
$Q_{\max}$	13.4	9.3	17.0	11.4	14.0	15.3	13.4 ± 2.75	62.5

[a] Cats 1, 2, and 3 weighed 2.9, 3.7, and 1.9 kg, respectively.

[b] The model is the concatenation of a cylindrical tube and an exponential horn and is described in Sec. III. To better describe the sharp minima and maxima observed in the model responses impedance, calculations were made at a density of 200 points/decade.

[c] The maximum magnitude of the impedance $|Z|_{\max}$ and the frequency of the maximum $f_{\max}$ were defined by interpolation from each magnitude versus frequency data plot. The impedance maximum was assumed to lie between the two largest magnitude values (which were always consecutive). A line was defined by the two points on the low-frequency side of the impedance maximum; a second line was defined by the two points on the high-frequency side. The intersection of these lines defined $|Z|_{\max}$ and $f_{\max}$.

[d] The Q's were calculated using the interpolated $f_{\max}$ and bandwidths at 3, 4.8, and 7 dB below the interpolated $|Z|_{\max}$; $Q_{\max} = (Q_{3\,\mathrm{dB}} + 2^{1/2}\,Q_{4.8\,\mathrm{dB}} + 2Q_{7\,\mathrm{dB}})/3$ (Guinan and Peake, 1967).

[e] The frequency of the minimum magnitude of the impedance that follows the maximum $f_{\min}$ was defined by the intersection points of lines defined by the four data points around the minimum. One line was defined by the two points on the low-frequency side. The second line was defined by the two points on the high-frequency side.

C. Effects of the configuration of the external ear

The freshly excised external ear is rigid enough to maintain its normal shape during the measurements. The configuration of the cartilaginous ear tube is most easily altered by rotating the pinna flange and concha about the canal–concha "joint" (A_3 in Fig. 7). This rotation approximates the most prominent motion of the concha and pinna flange when cats move their pinnae.

In order to assess the sensitivity of Z_E to variations in the configuration of the external ear, we introduced systematic variations in the flexure of the canal–concha joint. In our experimental arrangement, the ear was supported both by the acoustic assembly coupled to the tympanic ring and by strings that attached the pinna to a rigid frame (Fig. 2). The pinna flange and concha were moved relative to the canal by rotating the supporting frame relative to the acoustic assembly [Fig. 9(a)–(c)].

Measurements made before and after changes in the configuration of the external ear [Fig. 9(d)] show that Z_E is not greatly affected by rather large rotations in either direction, but an asymmetry is apparent in the magnitude of the changes. Over most of the frequency range, $|Z_E|$ is increased somewhat by backward rotation but is little affected by forward rotation. Our interpretation of this result is represented in the diagrams of Fig. 9(b) and (c). Backwards rotation of the external ear visibly constricts the canal–concha joint ["5" in Fig. 7(b)] to a size where its impedance presumably becomes large enough to increase the total impedance of the ear tube. Forward rotation, on the other hand, makes the joint opening larger [Fig. 9(c)], which presumably lessens an already small contribution of the joint impedance to Z_E. Similar rotation-induced changes were seen with all six ears.

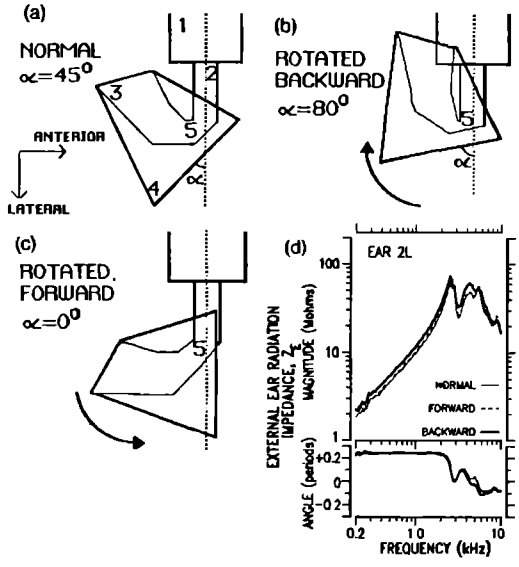

FIG. 9. Effects of alterations in the configuration of the external ear. The sketches of parts (a), (b), and (c) show schematically how the configuration of the external ear was altered by the experimental rotation of the pinna flange and concha. The view is of a right ear from above. The lines are a projection of the outline of the entire cartilaginous ear tube. The thinner lines would normally be hidden from view. The numbers label: (1) the acoustic assembly, (2) the canal, (3) the medioposterior edge of the concha, (4) lateroposterior edge of the pinna flange, and (5) the canal–concha joint. The dotted line is the long axis of the canal and acoustic assembly. The position of the pinna flange was measured by the angle α between the plane of the pinna-flange opening and the long axis of the canal. The rotations illustrated in (b) and (c) were produced by rotating the frame that supported the pinna flange. The diagrams represent our impressions of the resulting distortion of the ear. The measurements in (d) illustrate the sensitivity of Z_E to large changes in α (0°, 45°, and 80°). The normal and forward measurements are indistinguishable at most frequencies.

D. Effects of surgical alteration of the external ear

Gross surgical alterations of the external ear produced changes in Z_E that were similar in all six ears. Typical impedances measured after removal of the pinna flange and, again, after removal of the concha are illustrated in Fig. 10(a), and features of these measurements in the six ears are in Table II. Removal of the pinna flange (leaving the canal and concha) causes little or no change in the masslike low-frequency Z_E of all six ears (the mean change in $|Z_E|$ at 0.5 kHz is less than 1%). However, large changes occur in the middle and high frequencies, which can be accounted for by an upward shift in f_{max} and f_{min} and a dramatic increase in the prominence of the maxima and minima in $|Z_E|$. Also, the angle of Z_E after pinna-flange removal is far from 0 at most frequencies and changes rapidly with frequency near the frequencies of the magnitude extrema. The changes in the magnitude extrema and angles produced by pinna-flange removal suggest a large decrease in damping. Removal of the concha reduces the masslike low-frequency $|Z_E|$ by about 30% and further increases the magnitude and frequency of the impedance maximum in each ear.

The real part of Z_E plays a key role in the performance of the external ear (see Sec. III). Figure 10(b) illustrates $\mathrm{Re}\{Z_E\}$ in an intact and surgically altered ear. Differences

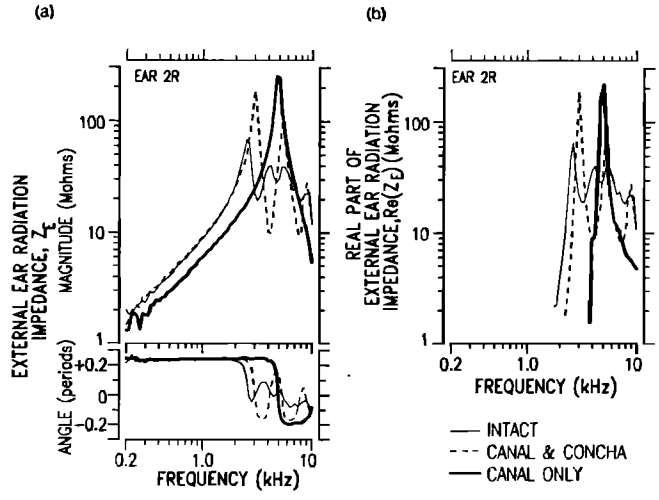

FIG. 10. Radiation impedance measured in one ear (2R), before surgical modification (intact), after removal of the pinna flange (canal and concha), and after removal of the concha (canal only). (a) Magnitude and angle of the impedance. (b) The real parts $\mathrm{Re}\{Z_E\}$'s of the impedances calculated from the data in (a). As was discussed in Sec. I, the accuracy of real-part estimation deteriorates as the impedance angle approaches 0.25 periods. The $\mathrm{Re}\{Z_E\}$'s in (b) are only plotted at frequencies greater than the low-frequency limit above which they rise monotonically to their maximum.

in the $\mathrm{Re}\{Z_E\}$'s of the three external-ear conditions are readily apparent. In all conditions in the low-frequency range, $\mathrm{Re}\{Z_E\}$ decreases rapidly as frequency decreases; the effect of the presence of the pinna flange and concha is to lower the frequency where the rapid decrease in $\mathrm{Re}\{Z_E\}$ begins. The pinna flange also smooths out the rapid fluctuations of $\mathrm{Re}\{Z_E\}$ with frequency that are observed when the pinna flange is removed.

III. DISCUSSION

A. Possible effects of the head and body on Z_E

Our measurement arrangement differs from the natural situation in that the external ear is removed from the head. Three lines of evidence argue against any large contribution of the head and body to the magnitude or angle of Z_E over the frequency range of our measurements. First, measurements at frequencies between 0.2 and 2 kHz show little effect of pinna-flange removal on the magnitude and angle of Z_E [Fig. 10(a)]; it is unlikely then that the more remote head and body have a large effect in this frequency range. Second, at higher frequencies (above 2 kHz), the pinna flange and concha impart a directionality to the ear that enhances the coupling of sounds from the anteroipsilateral direction to the tympanic membrane (Wiener *et al.*, 1966; Phillips *et al.*, 1982). By the reciprocity principle, the radiation of sound at these high frequencies will be concentrated laterally and anteriorly, thereby reducing the interaction of the head and body with the radiated sound. The third argument against any large head-and-body effects on Z_E comes from our model analysis. The magnitude and angle of the radiation impedance of a tube-and-horn model of the cat external ear (described in the next section) are only moderately altered when the opening of the horn is surrounded by an infinite baffle. The baffle-induced alterations in $|Z_E|$ are less than 5% at frequencies below 2.5 kHz, and are generally less than 20% at higher frequencies (the largest change, a difference of 50% in $|Z_E|$, occurs at the frequency of the maximum impedance magnitude). The effects of the head and body on Z_E are likely to be smaller than the effect of such a baffle.

Even though the effect of the head and body on the magnitude and angle of Z_E is small, it is conceivable that they have larger effects on $\mathrm{Re}\{Z_E\}$, especially at frequencies below 2 kHz, where the angle is near 0.25 periods, $\mathrm{Re}\{Z_E\} \ll |Z_E|$, and large changes can occur in the real part without apparant change in $|Z_E|$. Our analysis indicates that placing an infinite baffle around the opening of a tube-and-horn model of the external ear increases $\mathrm{Re}\{Z_E\}$ by a factor of 2 at frequencies below 2 kHz and has smaller effects on $\mathrm{Re}\{Z_E\}$ at higher frequencies. The effects of the head and body on $\mathrm{Re}\{Z_E\}$ should be smaller than the baffle effect.

B. Relationship of Z_E to external-ear structure: A simple model

Models for the acoustic behavior of the external ear have generally assumed that the walls of the cartilaginous ear tube are effectively rigid, and, therefore, the shape of the tube determines its acoustic behavior (Wiener and Ross, 1946; Wiener *et al.*, 1966; Shaw and Teranishi, 1968; Teranishi and Shaw, 1968; Hudde, 1983; Stinson, 1985). One way to test the validity of this assumption is to determine whether the dependences of Z_E on frequency and structural modifications (Fig. 10) are duplicated by the impedance of a rigid-walled model of the same shape.

Since we have measurements of dimensions of the external-ear tube from each of our six ears, we tested whether interear variations in structure could be related to the interear variations in Z_E. For example, simple acoustic theory suggests a negative correlation between the length of the canal and the f_{max} of the canal-only impedance measurement. The canal length should be approximately a quarter of the wavelength at this frequency. At the average f_{max}, 5.37 kHz, $\lambda/4 = 16.1$ mm, which is between the mean values of L_1 (9.5 mm) and L_2 (18.9 mm). However, we found no significant correlation between the individual f_{max}'s and either L_1, L_2, or the mean of these lengths. The reasons for the lack of correlation are not clear; apparently, our length measurements are not completely accurate representations of the acoustic length of the canal. Possible reasons for the discrepancies are: (1) The effective length of the canal is affected by the variations in the cross-sectional shape and area of the canal tube; (2) the silastic impressions we used in our measurements may not maintain the precise shape of the ear; and (3) as previously described, the anatomical measurements involve subjective judgments that lead to variations between repeated measurements of as much as 10%. These inaccuracies, coupled with the relatively small interear variations observed in the impedance measurements, make it difficult to correlate ear structure and impedance. Because of this problem, we have not tried to represent interear variations in our model. Rather, as this is a first step toward the determination of the structural basis of the impedance measurements, we developed a model that is consistent with the average dimensions of the six external ears and has the main features observed in all of the impedance measurements.

The model configuration consists of a uniform circular tube abutting an exponential horn [Fig. 11(a)]. This model has four parameters (the lengths of the uniform and exponential sections, area of the uniform tube, and the horn constant) that were chosen to be roughly consistent with the anatomical measurements of Table I and to fit the impedance measurements. The first step in the construction of the model was to fit the uniform tube to the canal's anatomical and impedance measurements. Then, an exponential horn was attached to the tube and the horn's dimensions were adjusted to fit both the impedances of the canal and concha configuration and the intact ear. The primary criterion used to judge the fit was the agreement of the frequencies of the impedance maxima. The second (almost equally important) criterion was that the cross-sectional areas of the model approximate those of the ear. The third (and least important) criterion was the agreement between the low-frequency impedance magnitudes. A close fit was readily achieved between the tube model and canal-only measurements. With the model horns, it was difficult to fulfill the first two criteria without causing some disagreement in the third.

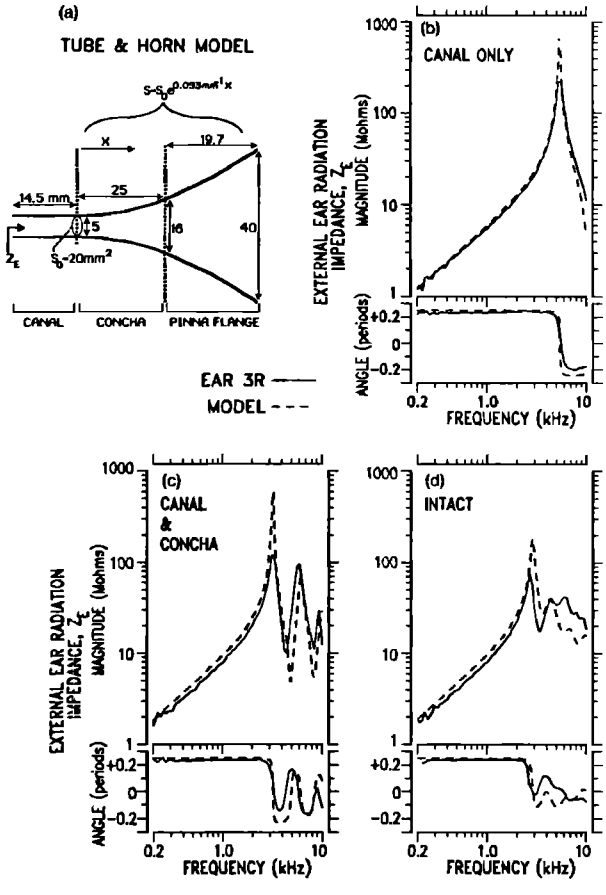

FIG. 11. Comparison of the measured radiation impedances of a typical external ear (3R) with the theoretical impedances of a model consisting of a cylindrical tube and a finite exponential horn. (a) Cross section of the model. The dotted lines separate the model into canal, concha, and pinna-flange sections. The canal is modeled as a lossless uniform tube. The concha and pinna flange are modeled as a lossless exponential horn. (All linear dimensions are in mm.) S is the cross-sectional area of the horn. (b) Comparison of measurements and model for the radiation impedance of the canal only condition. (c) Comparison of canal and concha measurement and model. (d) Comparison for the intact ear.

Consider, first, the uniform tube model of the canal-only condition. In Fig. 11(b), the Z_E for an isolated canal is compared to the radiation impedance looking through a cylindrical tube terminated with the radiation impedance of a circular opening with uniform velocity distribution.[6] The tube's length was fixed by the frequency of the impedance maximum, and the area was selected to yield the correct low-frequency mass. The resulting length (14.5 mm) is nearly equal to the average canal length, and the cross-sectional area of the model tube (20 mm^2) closely approximates the mean minimum cross-sectional area of the six canals (Table I). There is good agreement between model and measurement over most of the frequency range. However, the model's maximum $|Z_E|$ and Q are much larger than the measurements' (the model's $|Z|_{max}$ and Q_{max} are 1533 MΩ and 62.5, while the means of these features in the measurements are 322 MΩ and 13.4, Table II). These large discrepancies indicate that the damping in the model is too small and suggest that, in the real canal, energy is lost through mechanisms that are not included in the model.

In Fig. 11(c), the Z_E of a canal and concha is compared with the radiation impedance of the tube plus a "short" exponential horn.[7] The length of the horn (25 mm) is about equal to the mean maximum length of the concha (Table I): the cross-sectional area of the horn throat (20 mm^2) is identical to the area of the tube. The horn constant (0.093 mm^{-1}) has been chosen to yield an area at the mouth of the horn (205 mm^2), which is a little smaller than the mean area of the concha opening (Table I). The impedance of this model shows a pattern of maxima and minima similar to the canal and concha measurements, but the $|Z|_{max}$ and Q_{max} produced by the model are again much larger than those of the measurements.

Figure 11(d) is a comparison of the radiation impedances of an intact external ear and a tube and longer-horn model. The area of the mouth of the horn (1280 mm^2) is effectively identical to measurements of the pinna-flange area. The Z_E's of the ear and model are slightly different in low-frequency magnitude and in f_{max} (Table II), and both are approximately resistive at frequencies above the maximum. However, the maximum magnitude and Q of the model are again larger than those of the measurement.

Thus a rigid-walled tube and exponential-horn model [Fig. 11(a)] produces impedances that are similar to the measurements in many ways. The most prominent differences appear to result from losses that are not included in the model. Possible sources of these losses are complexities in the shape of the ear that were not included in the model, nonrigid behavior of the external-ear walls, and viscous and thermal losses.

C. Comparison of Z_E and Z_T for cat

The effects of the middle ear on the acoustic performance of the external ear, and of the external ear on the performance on the middle ear, are determined by the input impedance of the middle ear Z_T and the radiation impedance Z_E. The equivalent circuit in Fig. 12 represents this interaction. The sound pressure at the tympanic membrane P_T can be represented as the sum of two components:

$$P_T = (1 + Z_E/Z_T)^{-1}P_{TB} + (1 + Z_T/Z_E)^{-1}P_{TE}. \quad (2)$$

The first term on the right side of Eq. (2) is the component of P_T produced by external sound sources and the second term is the component produced by internal sound sources (e.g., otoacoustic emissions). With excitation of the external ear by either external or internal sources, the ratio of the two impedances influences the resultant sound pressure at the tympanic membrane.

The data in Fig. 12 show that the relationship of Z_E to Z_T is highly frequency dependent. At frequencies below 1 kHz, $|Z_T|$ is at least six times larger than $|Z_E|$ ($|Z_T| > 6|Z_E|$) and, therefore, the sound pressure produced at the tympanic membrane by external sound sources is relatively independent of small changes in Z_T; i.e., $P_T \approx P_{TB}$. On the other hand, the component of P_T produced by sources within the ear is approximately proportional to Z_E and can

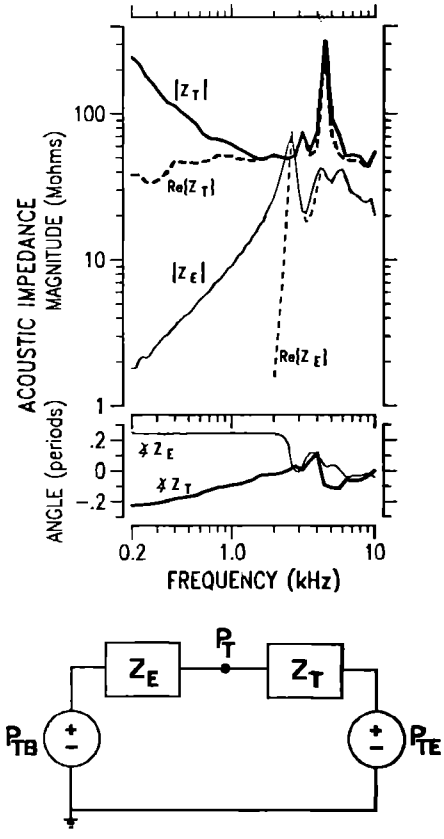

FIG. 12. A comparison of the mean Z_E of six ears (thin solid lines) and its real part, $\mathrm{Re}\{Z_E\}$ (thin dashed line), from the measurements of Fig. 8, and the mean middle-ear input impedance Z_T (thick solid lines), and it real part $\mathrm{Re}\{Z_T\}$ (thick dashed line), as determined by Lynch (1981). The Z_T measurements were obtained in five ears with the middle-ear cavities opened widely. To correct for this cavity modification, the mean of the measurements was multiplied by the ratio Z_T(intact cavities)/Z_T(opened cavities) measured in a typical ear. The large sharp peak in $|Z_T|$ near 4.5 kHz results from the middle-ear cavities. The equivalent circuit (same as in Fig. 1) represents the dependence of sound pressure at the tympanic membrane P_T on Z_E and Z_T.

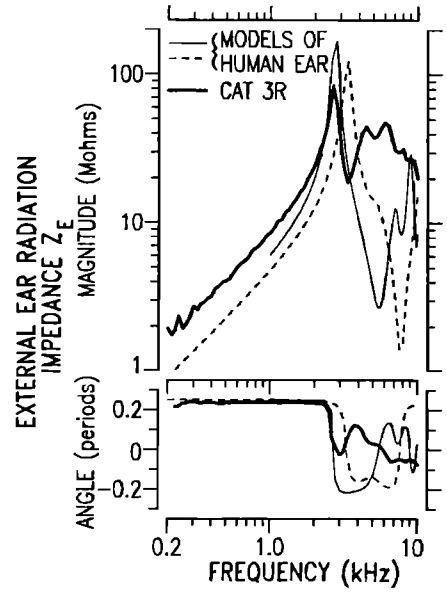

FIG. 13. The radiation impedance of a cat ear (3R), a physical model of the human external ear (thin solid line; Shaw, 1976), and a mathematical model of the human ear (thin dashed line; Siebert, 1970, 1973). The impedance of the physical model, "the NRC model external ear," was measured with an impedance tube (Shaw, 1975, 1976, 1982); the model ear was mounted in a baffle. The mathematical model represents Z_E by the acoustic impedance looking out through two concatenated uniform tubes of different diameter. The opening of the larger outermost tube was flanged by an infinite baffle (Siebert, 1970, 1973).

be greatly increased if $|Z_E|$ is increased by blocking the ear canal. The influence of ear-canal blocking on the magnitude of low-frequency otoacoustic emissions has been noted previously (Kemp, 1979; Matthews, 1980; Rosowski *et al.*, 1984; Fahey and Allen, 1986). Above 1 kHz, the magnitudes of the Z_T and Z_E are more nearly equal with $|Z_T| \geq |Z_E|$ at most frequencies, and the P_T's produced by either external or internal sound sources will be influenced by changes in either one of the impedances.

The performance of the cat ear as an "impedance matcher" can also be assessed from Fig. 12. The impedances at the tympanic membrane are matched when Z_E and Z_T are of equal magnitude and opposite angle (i.e., complex conjugates). Below 1 kHz, the impedance magnitudes are very different and only a small fraction of the sound power available from an external source enters the middle ear. In the 2- to 10-kHz frequency range, the impedances are more nearly matched and 30% to 100% of the available power enters the middle ear. This issue is addressed elsewhere in more detail (Rosowski *et al.*, 1986).

D. Comparison of Z_E for cat and man

Several investigators have estimated the radiation impedance of the human external ear. Shaw (1976, 1982), Kuhn (1979), and Schroeter and Piesselt (1986) measured the radiation impedance of physical models of the external ear, and Siebert (1970, 1973) used a simple analytical model of two uniform tubes representing the concha and canal to calculate Z_E. The radiation impedance of all of these models of the human ear are similar. Shaw's and Siebert's estimates are compared with the measured Z_E of a cat ear in Fig. 13. For frequencies below f_{max}, all three curves have a masslike impedance. The larger impedance magnitude of the cat ear is roughly consistent with the differences in dimensions of canals and conchas of the two species. At higher frequencies, the most striking difference between the cat measurements and human models is the greater prominence of the models' maximum and minimum $|Z_E|$. The wide range in magnitude between maximum and minimum suggests a lack of damping in the human models and may reflect a difference between the Z_E of real external ears and the models rather than an interspecies difference. The model we used to approximate the cat ear also produces exaggerated extrema (Fig. 11). Furthermore, our measurements (Fig. 10) indicate that the pinna flange adds damping to the external ear. Siebert's model did not include a pinna flange representation, which may account for its relatively undamped Z_E. Shaw's model includes a geometrically simple representation of the pinna flange; a more complex representation might introduce more damping.

E. Radiation impedance and external-ear performance

When Z_E is measured with a sound source at the location of the tympanic membrane, the resulting sound field is radiated in all directions. Through the reciprocity principle, Z_E can be related to the receiving properties of the ear (Siebert, 1970, 1973; Shaw, 1976, 1979, 1988).

1. Mean-square pressure ratio T_T^2

The performance of the external ear has often been described (e.g., Shaw, 1974) in terms of the pressure ratio $|P_T(\phi,\theta)|/|P_{PW}|$, where P_T is the sound pressure at the tympanic membrane and P_{PW} is the sound pressure of an incident plane wave propagating in a direction specified by the angles ϕ and θ. The average of the square of this ratio over all source directions T_T^2 is primarily determined by Z_E and Z_T:

$$T_T^2 \equiv \frac{1}{4\pi a^2}\int_0^{2\pi} d\phi \int_0^{\pi} d\theta\, a^2 \sin\theta \left|\frac{P_T(\phi,\theta)}{P_{PW}}\right|^2 = \frac{\lambda^2}{\pi\rho c}\eta_R \,\mathrm{Re}\{Z_E\}\left|\frac{Z_T}{Z_E+Z_T}\right|^2, \quad (3)$$

where a is the hypothetical radius of the sphere over which the spatial average is computed (N.B.: the average is independent of a); λ is the sound wavelength; ρ is the density of air; c is the speed of sound; and η_R is the radiation efficiency of the external ear (presumably ≈ 1). This relation is derived in Shaw (1976, 1988) for the case of diffuse-field[8] stimulation, and the basic result is also described by Siebert (1970, 1973).

Siebert (1970) pointed out that Eq. (3) implies a kind of conservation principle. Any modification of the acoustic environment that increases $|P_T(\phi,\theta)|/|P_{PW}|$ for some direction, but does not alter Z_E, *must* also decrease $|P_T(\phi,\theta)|/|P_{PW}|$ for some other direction. Examples of this type of alteration might include movements of the pinna relative to the head (Calford and Pettigrew, 1984; Middlebrooks and Knudsen, 1987) and changes in the size of the head or the position of the body.

The relationship between Z_E and T_T^2 is simplified at low sound frequencies, where the sound wavelength λ is much greater than the dimensions of the external ear and head. In this case, Z_E is the radiation impedance of a "simple source" (e.g., Kinsler and Frey, 1962, p. 164) such that $\mathrm{Re}\{Z_E\} = \pi\rho c/(\lambda^2)$. The combination of this result with the assumption that $\eta_R = 1$ and the observation that $|Z_T| \gg |Z_E|$ in the low-frequency range (Fig. 12) leads to $T_T^2 \approx 1$ for low frequencies. This theoretical result is consistent with many experimental measurements of a near unity $|P_T(\phi,\theta)|/|P_{PW}|$ for all angles of incidence at low frequencies (see Shaw, 1974).

We can also estimate T_T^2 by averaging the square of the magnitude of measured pressure ratios $(|P_T(\phi,\theta)|/|P_{PW}|)^2$ made at many discrete azimuths ϕ's and elevations θ's distributed equally throughout space (e.g., Shaw and Teranishi, 1968; Shaw, 1974, 1976, 1982; Chan *et al.*, 1986), such that

$$T_T^2 \approx \left(\sum_{i=1}^{n}\left|\frac{P_T(\phi,\theta)}{P_{PW}}\right|^2\right)\frac{1}{n}, \quad (4)$$

where n is the number of source positions over which the measurements are averaged.

Shaw (1976) estimated T_T^2 from measurements of P_T for 52 source locations distributed uniformly on a hemisphere around a model of a human ear in a plane baffle. He compared this computation to the prediction from Eq. (3) (assuming $\eta_R = 1$) using measurements of Z_E and Z_T made on the same model. The computed and measured results are very similar over the frequency range of the measurements (2–15 kHz); with significant differences only at some maxima. These small differences led Shaw to suggest that η_R is somewhat less than 1 (≈ 0.8) for these conditions. Kuhn (1979), using measurements made with an anthropomorphic manikin with external ears made from an impression of a human ear, has similarly compared measurements and calculations of T_T^2 and shows differences of 2 dB between the two. These data suggest that $\eta_R \geqslant 0.6$.

The curves in Fig. 14 allow a comparison of $T_T(T_T^2)^{1/2}$ calculated either from Eq. (3) (with $\eta_R = 1$) using measurements of Z_E and Z_T or, from Eq. (4), with the $|P_T(\phi,\theta)|/|P_{PW}|$ measurements made at five different source directions by Wiener *et al.* (1966). Even though the sampling of the spatial dependence in the $|P_T(\phi,\theta)|/|P_{PW}|$ measurements is both sparse and nonuniform, the two curves are similar. One would like to use the differences between the two curves in Fig. 14 to determine whether η_R deviates appreciably from unity, but the shortcomings of the spatial sampling in the $|P_T(\phi,\theta)|/|P_{PW}|$ measurements preclude any conclusion about the loss of acoustic power within the cat external ear.

2. Diffuse-field absorption cross section A_{DF}

The efficacy of a receiver of radiation is often measured in terms of an "effective area" or "absorption cross section"

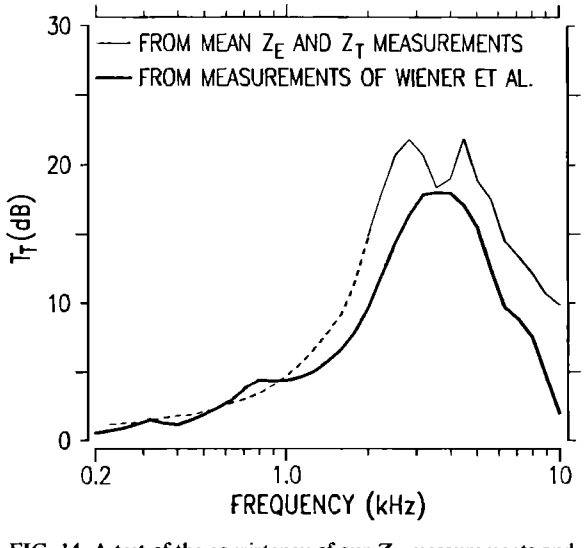

FIG. 14. A test of the consistency of our Z_E measurements and measurements of the external ear sound-pressure ratio. Calculations of the square root of the spatial average of the squared pressure ratio T_T, obtained with (1) Eq. (3) assuming $\eta_R = 1$ and the Z_E and Z_T data of Fig. 12, and (2) Eq. (4) and measurements of external-ear pressure transformations (Wiener *et al.*,1966, Fig. 4). With Eq. (3), model estimates of $\mathrm{Re}\{Z_E\}$ were used at frequencies below 2 kHz (the dashed portion of the curve).

defined as the ratio of power received to power per unit area in the incident wave. For a uniform plane wave incident on an ear, the *absorption cross section* A is a function of the direction of propagation of the incident wave, such that

$$A = \rho c \left| \frac{P_T(\phi,\theta)}{P_{PW}} \right|^2 \frac{\mathrm{Re}\{Z_T\}}{|Z_T|^2} \tag{5}$$

(e.g., Rosowski *et al.*, 1986). Shaw (1979, 1988; Shaw and Stinson, 1983) has combined this concept with that of a diffuse acoustic field and has defined the *diffuse-field absorption cross section* A_{DF} as the ratio of power delivered to the middle ear divided by the power density in the diffuse field:

$$A_{DF} = \eta_R \frac{\lambda^2}{4\pi} \left(\frac{4\mathrm{Re}\{Z_E\}\mathrm{Re}\{Z_T\}}{|Z_E + Z_T|^2} \right). \tag{6}$$

The term in large parentheses on the right side of Eq. (6) is the ratio of the sound power delivered to the middle ear divided by the maximum power available; we call this quantity the *power utilization ratio* or PUR (Rosowski *et al.*, 1986). When Z_E and Z_T are matched, PUR = 1, and, if $\eta_R = 1$, then A_{DF} equals its theoretical maximum $A_{DF,ideal} = \lambda^2/4\pi$.

The measurements of Z_E and Z_T for cat (Fig. 12) can be used to compute A_{DF}, with the assumption that $\eta_R = 1$ (Fig. 15). Since Z_E and Z_T differ greatly at low frequencies, but come close to matching above 2 kHz (Fig. 12), A_{DF} is far less than ideal ($< 0.01\lambda^2/4\pi$) at frequencies below 1 kHz (indicating a large "mismatch" between Z_E and Z_T) and within a factor of 3 of the ideal at frequencies above 2.5 kHz.

At 2.8 kHz, the frequency at which the cat's ear absorbs sound most effectively, the computed A_{DF} ($\approx 1200\ \mathrm{mm}^2$) is nearly ideal and of a magnitude approximately equal to the area of the pinna-flange opening (Table I). This approximate equality of the peak A_{DF} and the area of the pinna-flange opening suggests a simple association of external-ear anatomy and physiology, but this association is not consistent with all of our data. For example, the A_{DF}'s computed from the Z_E's measured after removal of the pinna flange and concha (Fig. 10, Table II) are three to four times larger than the appropriate anatomical areas (Table I). (The peak A_{DF} computed for the canal and concha condition is 700 mm^2 compared to the average A_4 of 232 mm^2, while the peak A_{DF} computed for the canal only condition is 150 mm^2 compared to the average A_3 of 37 mm^2.) Therefore, rules that relate receiver cross section to anatomical area have to be more complicated. These area computations also clearly illustrate that the cat pinna flange and concha improve the power-collection capabilities of the ear as well as contribute to the ears spatial selectivity.

Also included in Fig. 15 is a human A_{DF} estimate calculated from Shaw's (1976) model measurements of Z_E and Hudde's (1983) and Rabinowitz's (1981) Z_T measurements. This estimate of A_{DF} for the human ear, which is similar to that reported by Shaw and Stinson (1983), is generally lower than the cat estimate, has a peak at 45% of the theoretical ideal near 2.5 kHz, and comes closest to the ideal at 7 kHz. Comparison of the curves in Fig. 15 suggests that, between 2–10 kHz, the cat external and middle ear is a better collector of sound power than the human ear. However, it should be remembered that the estimate of A_{DF} is dependent on knowledge of $\mathrm{Re}\{Z_E\}$, and we have suggested that estimates of Z_E based on simple models of the external ear underestimate $\mathrm{Re}\{Z_E\}$ and, therefore, will lead to underestimates of A_{DF}.

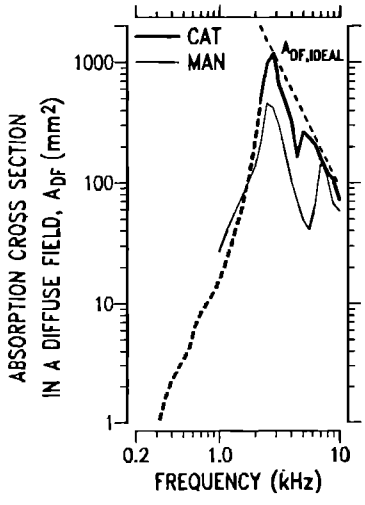

FIG. 15. Diffuse-field absorption cross section A_{DF} for cat and man calculated from Eq. (6) (with the assumption that $\eta_R = 1$). The data of Fig. 12 were used to define Z_E and Z_T for cat. The thick dashed line delimits the low-frequency range in which the model estimate of $\mathrm{Re}\{Z_E\}$ was used in the calculations (as in Fig. 14). The human A_{DF} was calculated from Shaw's (1976) model measurements of Z_E and Rabinowitz's (1981) and Hudde's (1983) measurements of Z_T. The thin dashed line is $A_{DF,ideal} = \lambda^2/4\pi$.

F. Approaches to comparative measurements of external-ear performance

The results that we have discussed here suggest approaches to the measurement of acoustic behavior of the external ear that may make the collection and comparison of measurements across a wide range of species more practical. First, in comparisons of external-ear function across species, performance as a power collector can be separated from spatial selectivity (Siebert, 1970, 1973; Khanna and Tonndorf, 1978) by the use of the diffuse-field absorption cross section A_{DF} (or the power utilization ratio), which can be determined (assuming $\eta_R = 1$) from measurements of two acoustic impedances, Z_E and Z_T (see footnote 9). These measurements are independent of the source direction and do not require (apparently) an anechoic room. Knowledge of A_{DF} allows comparison of ears to each other and to an ideal receiver. A possible complication in this approach is that the radiation efficiency η_R must be known. This problem would be alleviated if it can be demonstrated that η_R is generally close to one.

Other measures such as a "directivity factor" (e.g., Beranek, 1949, pp. 647–561) or "optimal area" (Phillips *et al.*, 1982; Middlebrooks and Knudsen, 1987) might be used to assess spatial selectivity. These measures do not depend on

the middle ear (Hudde and Schroeter, 1980), and measurements could be obtained with the tympanic membrane blocked. Such a constraint could be experimentally helpful in that directivity measurements need not be carried out on *live* animals. Indeed, an accurate physical model of the external ear and head would provide satisfactory results. The use of such models would make measurements over many angles of incidence much easier, since the state of the "animal" would not vary. Also, the measurements could be made in well-controlled acoustic conditions and structural modifications could be made and reversed easily.

We suggest that these approaches can expedite the collection and comparison of interspecies external-ear performance measurements. When such results are available, we can begin to relate the acoustic function of the external ear to the behavior of animals (Griffin, 1958; Batteau, 1967; Shaw, 1974, 1982; Heffner *et al.*, 1982; Lawrence and Simmons, 1982; Blauert, 1983; Coles and Guppy, 1986).

ACKNOWLEDGMENTS

We thank R. A. Eatock, D. R. Ketten, N. Y.-S. Kiang, J. B. Kobler, W. M. Rabinowitz, and T. F. Weiss for their comments on earlier versions of this manuscript, and C. M. Gabriele, P. J. Davis, and the staff of the Eaton–Peabody Laboratory for assistance with the measurements and manuscript preparation. We also thank E. A. G. Shaw and W. M. Siebert for instructive exchanges as well as comments on the manuscript. This work was supported by NIH Grants 5-PO1-NS-13126 and 5-RO1-NS-18682 and by the M.I.T. Undergraduate Research Opportunity Program (LHC).

[1]For example, the large pinna flanges of the external ears of rabbits and elephants are thought to play a role in thermoregulation (Hammel, 1968; Buss and Estes, 1971).

[2]Relatively small effects of the torso and its covering have also been shown in humans (Burkhard and Sachs, 1975; Kuhn, 1977, 1979).

[3]The cylindrical 5-mm^3 cavity was made of Plexiglas with an inner diameter $2a$ of 4 mm and a length L of 0.139 mm. The cavity's acoustic input impedance was assumed to equal $-jpc\cot(L\omega/c)/(\pi a^2)$. The transmission line was a cylindrical copper tube with a 4.8-mm i.d. and length of 10.9 m, which was terminated with an acoustic resistor of an impedance equal to the tube's characteristic impedance. The input impedance of the transmission line was assumed to equal its characteristic acoustic impedance $\rho c/(\pi a^2)$. We have explored more complex models for the calibration impedances, which include losses caused by viscosity and heat conduction (White *et al.*, 1980). Use of these lossy models would change the impedances reported here by less than 3% in magnitude and 0.01 periods in angle.

[4]We use "cartilaginous ear tube" to refer to the walls of the air-filled passage of the exernal ear.

[5]The anatomical nomenclature is similar to that used by Shaw (1974) to describe the human external ear.

[6]The radiation impedance of the tube was determined by first calculating the radiation impedance of a circular opening at the end of a long tube where the area of the opening is equal to the tube's cross section (Beranek, 1954, p. 123). In performing this calculation, we assume a uniform velocity distribution across the opening. This radiation impedance was then used as the terminating impedance of the cylindrical, lossless, uniform tube (Kinsler and Frey, 1962, eqn. 8.35).

[7]The radiation impedance of a horn plus a tube was calculated by first determining the radiation impedance of a circular opening in a long tube of area equal to the area of the mouth of the horn. This radiation impedance was then used as the terminating impedance of a finite exponential horn (Malecki, 1969, p. 469), and the impedance at the throat of the horn was calculated. Finally, the throat impedance of the horn was used to terminate a uniform tube (Kinsler and Frey, 1962, eqn. 8.35). These calculations assume that the tube and horn are lossless.

[8]In a diffuse field, "incoherent" sound sources are dispersed in space so that at any point in space the *temporal* mean of the square pressure that results from *all* the sources is the sum of the mean-square pressures produced by each source acting alone (see, e.g., Beranek, 1949, p. 645; Pierce, 1981, p. 72.

[9]"Source" and "load" impedances at locations other than the tympanic membrane may be equally useful for this purpose, e.g., the impedance looking in and out from the entrance of the ear canal (Hudde and Schroeter, 1980).

Batteau, D. W. (**1967**). "The role of the pinna in human localization," Proc. R. Soc. London Ser. B **168**, 158–180.

Beranek, L. L. (**1949**). *Acoustic Measurements* (Wiley, New York).

Beranek, L. L. (**1954**). *Acoustics* (McGraw-Hill, New York).

Blauert, J. (1983). *Spatial Hearing* (MIT, Cambridge, MA).

Burkhard, M. D., and Sachs, R. M. (**1975**). "Anthropometric manikin for acoustic research," J. Acoust. Soc. Am. **58**, 214–222.

Buss, I. O., and Estes, J. A. (**1971**). "The functional significance of movements and positions of the pinnae of African elephants, *Loxodonta africana*," J. Mammal. **52**, 21–27.

Calford, M. B., and Pettigrew, J. D. (**1984**). "Frequency dependence of directional amplification at the cat's pinna," Hear. Res. **14**, 13–19.

Chan, J. C. K., Musicant, A. D., and Hind, J. E. (**1986**). "Directional properties of the cat external ear," The IUPS Satellite Symposium on Hearing: Binaural Interactions and Sound Localization Representation, San Francisco, CA.

Coles, R. B., and Guppy, A. (**1986**). "Biophysical aspects of directional hearing in the Tammar wallaby, *Macropus eugenii*," J. Exp. Biol. **121**, 371–394.

Dear, S. P. (**1987**). "Impedance and sound transmission in the auditory periphery of the chinchilla," Ph.D. thesis, University of Pennsylvania, Philadelphia, PA.

Drescher, D. G., and Eldredge, D. H. (**1974**). "Species differences in cochlear fatigue related to acoustics of outer and middle ears of guinea pig and chinchilla," J. Acoust. Soc. Am. **56**, 929–934.

Fahey, P. F., and Allen, J. B. (**1986**). "Characterization of cubic intermodulation distortion products in the cat external auditory meatus," in *Peripheral Auditory Mechanisms*, edited by J. B. Allen, J. L. Hall, A. Hubbard, S. T. Neely, and A. Tubis (Springer, New York), pp. 314–321.

Griffin, D. R. (**1958**). *Listening in the Dark* (Yale. U. P., New Haven, CT).

Guinan, J. J., Jr., and Peake, W. T. (**1967**). "Middle-ear characteristics of anesthetized cats," J. Acoust. Soc. Am. **41**, 1237–1261.

Hammel, H. T. (**1968**). "Regulation of the internal body temperature," Ann. Rev. Physiol. **30**, 641–710.

Heffner, R., Heffner, H., Stichman, N. (**1982**). "Role of the elephant pinna in sound localization," Animal Behav. **30**, 628–629.

Hudde, H. (**1983**). "Measurement of the eardrum impedance of human ears," J. Acoust. Soc. Am. **73**, 242–247.

Hudde, H., and Schroeter, J. (**1980**). "The equalization of artificial heads without exact replication of the eardrum impedance," Acoustica **44**, 301–307.

Kemp, D. T. (**1979**). "Evidence of mechanical nonlinearity and frequency selective wave amplification in the cochlea," Arch. Otorhinolaryngol. **224**, 37–45.

Khanna, S. M., and Tonndorf, J. (**1978**). "Physical and physiological principles controlling auditory sensitivity in primates," in *Neurobiology of Primates*, edited by R. Noback (Plenum, New York), pp. 23–52.

Kinsler, L. E., and Frey, A. R. (**1962**). *Fundamentals of Acoustics* (Wiley, New York).

Kuhn, G. F. (**1977**). "Model for the interaural time differences in the azimuthal plane," J. Acoust. Soc. Am. **62**, 157–167.

Kuhn, G. F. (**1979**). "The pressure transformation from a diffuse sound field to the external ear and to the head and body surface," J. Acoust. Soc. Am. **65**, 991–1000.

Lawrence, B. D., and Simmons, J. A. (**1982**). "Echolocation in bats: The external ear and perception of the vertical positions of targets," Science **218**, 481–483.

Lynch, T. J., III (**1981**). "Signal processing by the cat middle ear: Admittance and transmission, measurements and models," Sc.D. thesis, MIT, Cambridge, MA.

Malecki, I. (**1969**). *Physical Foundations of Technical Acoustics* (Pergamon, Oxford).

Matthews, J. W. (1980). "Mechanical modeling of nonlinear phenomena observed in the peripheral auditory system," Sc.D. thesis, Washington University, St. Louis, MO.
Mehrgardt, S., and Mellert, V. (1977). "Transformation characteristics of the external human ear," J. Acoust. Soc. Am. 61, 1567–1576.
Middlebrooks, J.C., and Knudsen, E. I. (1987). "Changes in external ear position modify spatial tuning of auditory units in cat's superior colliculus," J. Neurophysiol. 57, 672–687.
Phillips, D. P., Calford, M. B., Pettigrew, J. D., Aitkin, L. M., and Semple, M. N. (1982). "Directionality of sound pressure transformation at the cat's pinna," Hear. Res. 8, 13–28.
Pierce, A. D. (1981). *Acoustics: An Introduction to Its Physical Principles and Applications* (McGraw-Hill, New York).
Rabinowitz, W. M. (1981). "Measurement of the acoustic input immitance of the human ear," J. Acoust. Soc. Am. 70, 1025–1035.
Rosowski, J. J., Carney, L. H., Lynch, T. J., III, and Peake, W. T. (1986). "The effectiveness of external and middle ears in coupling power into the cochlea," in *Peripheral Auditory Mechanisms*, edited by J. B. Allen, J. L. Hall, A. Hubbard, S. T. Neely, and A. Tubis (Springer, New York), pp. 3–12.
Rosowski, J. J., Peake, W. T., and Lynch, T. J., III (1984). "Acoustic input-admittance of the alligator-lizard ear: Nonlinear features," Hear. Res. 16, 205–223.
Rosowski, J. J., Peake, W. T., and White, J. R. (1984). "Cochlear nonlinearities inferred from two-tone distortion products in the ear canal of the alligator lizard," Hear. Res. 13, 141–158.
Saunders, J. C., and Garfinkle, T. J. (1982). "Peripheral physiology of the mouse ear," in *Auditory Psychobiology of the Mouse*, edited by J. F. Willot (Thomas, Springfield, IL).
Schroeter, J., and Poesselt, C. (1986). "The use of acoustical test fixtures for the measurement of hearing protector attenuation. Part II: Modeling the external ear, simulating bone conduction, and comparing test fixture and real-ear data," J. Acoust. Soc. Am. 80, 505–527.
Shaw, E. A. G. (1974). "The external ear," in *Handbook of Sensory Physiology: Vol. V/1: Auditory System*, edited by W. D. Keidel and W. D. Neff (Springer, New York), pp. 455–490.
Shaw, E. A. G. (1975). "The external ear: New knowledge," Scand. Audiol. Suppl. 5, 24–50.
Shaw, E. A. G. (1976). "Diffuse field sensitivity of the external ear based on the reciprocity principle," J. Acoust. Soc. Am. Suppl. 1 60, S102.
Shaw, E. A. G. (1979). "Performance of the external ear as a sound collector," J. Acoust. Soc. Am. Suppl. 1 65, S9.
Shaw, E. A. G. (1982). "1979 Rayleigh Medal Lecture: The elusive connection," in *Localization of Sound: Theory and Applications*, edited by R. W. Gatehouse (Amphora, Groton, CT), pp. 13–29.
Shaw, E. A. G. (1988). "Diffuse field response, receiver impedance, and the acoustical reciprocity principle," J. Acoust. Soc. Am. 84 (to be published).
Shaw, E. A. G., and Stinson, M. R. (1983). "The human external and middle ear: Models and concepts," in *Mechanics of Hearing*, edited by E. de Boer and M. A. Viergever (Nijhoff, Delft U. P., Delft, The Netherlands), pp. 3–10.
Shaw, E. A. G., and Teranishi, R. (1968). "Sound pressure generated in an external-ear replica and real human ears by a nearby point source," J. Acoust. Soc. Am. 44, 240–249.
Siebert, W. M. (1970). "Simple model of the impedance matching properties of the external ear," Q. Prog. Rep. No. 96, Research Laboratory of Electronics, MIT, Cambridge, MA, pp. 236–242.
Siebert, W. M. (1973). "Hearing and the ear," in *Engineering Principles in Physiology, Vol. 1* (Academic, New York), pp. 139–184.
Sinyor, A., and Laszlo, C. A. (1973). "Acoustic behavior of the outer ear of the guinea pig and the influence of the middle ear," J. Acoust. Soc. Am. 54, 916–921.
Stinson, M. R. (1985). "The spatial distribution of sound pressure within scaled replicas of the human ear," J. Acoust. Soc. Am. 78, 1596–1602.
Teranishi, R., and Shaw, E. A. G. (1968). "External ear acoustic models with simple geometry," J. Acoust. Soc. Am. 44, 257–263.
Vér, I. L., Brown, R. M., and Kiang, N. Y.-S. (1975). "Low-noise chambers for auditory research," J. Acoust. Soc. Am. 58, 392–398.
Von Bismark, G. (1967). "The sound pressure transformation function from free-field to the eardrum of chinchilla," M.S. thesis, MIT, Cambridge, MA.
Von Bismark, G., and Pfeiffer, R. R. (1967). "On the sound pressure transformation from free field to eardrum of chinchilla," J. Acoust. Soc. Am. 42, 1156.
White, R. E. C., Studebaker, G. A., Levitt, H., and Mook, D. (1980). "The application of modelling techniques to the study of hearing aid acoustic systems," in *Acoustical Factors Affecting Hearing Aid Performance*, edited by G. A. Studebaker and I. Hochberg (University Park, Baltimore, MD), pp. 267–296.
Wiener, F. M., Pfeiffer, R. R., and Backus, A. S. N. (1966). "On the sound pressure transformation by the head and auditory meatus of the cat," Acta Otolaryngol. 61, 255–269.
Wiener, F. M., and Ross, D. A. (1946). "The pressure distribution in the auditory canal in a progressive sound field," J. Acoust. Soc. Am. 18, 401–408.
Zurek, P. M. (1985). "Acoustic emissions from the ear: A summary of results from humans and animals," J. Acoust. Soc. Am. 78, 340–344.